

# Characterization of variability in 2-dimensional particle geometry via 3D structured light scanning

Chang Hoon Lee<sup>a</sup>, Seung Jae Lee<sup>b</sup>, Moochul Shfin<sup>a,\*</sup>

<sup>a</sup> Western New England University, Springfield, MA 01119, United States

<sup>b</sup> Florida International University, Miami, FL 33174, United States



## ARTICLE INFO

### Keyword:

3D structured light scanning  
Digital image analysis  
Morphology  
Regularity  
Roundness  
Sphericity

## ABSTRACT

In the characterization of the particle morphology via 2D digital image processing, image acquisition needs to be done in proper ways. Otherwise, the resulting parameters are significantly influenced by the procedures. This research characterizes potential variations that can mislead the interpretation of the 2D particle morphology parameters such as sphericity, roundness, and regularity indices depending on a projection angle at which a 2D image is taken. Besides, the 2D parameters are compared to Wadeffl's "true sphericity" evaluated using a 3D particle model obtained by 3D structured light scanning technology. The resulting variance in the 2D parameters is high, producing approximately more than 0.5 of variance depending on particles, the definition of the mineral parameters, and projection angles. The variations demonstrated in this research could provide additional insight to the 2D indices by considering 3D particle morphology indices.

## 1. Introduction

The characterization of particle morphology is of great importance in many disciplines including geology [1–3], biology [4], environmental engineering [5,6], nano-particles [7,8], and construction materials [9–11]. A variety of morphology indices have been developed to better characterize the shapes of aggregate at different length scales [12–16] along with the advances in image acquisition technologies such as laser scanner, scanning electron microscope, computed tomography [17–19], and simply 2-D digital imaging systems [20–22]. Despite the advances in the 3D imaging technologies, a 2D digital image-based analysis has been widely used because of its practicality and cost-effectiveness. However, a high degree of variability existing in 2D image analyses is produced by procedures (e.g., how many images are taken), while its influence on the result has not been highlighted well. Specifically, images of one particle (e.g., natural or crushed aggregate) taken at various projection angles typically appear differently, and those discrepancies can become more apparent when the shape of particles is elongated or flat. This implies there are some levels of variations in the quantified morphology indices depending on the angles at which each image is taken. However, a study of the variation in 2D morphology indices by using a physical camera is technically challenging for precisely controlling different projection angles as an example. Currently, stereoscopy [23–25] with a 3D scanner

becomes more popular, enabling one to obtain high-resolution 3D meshes for a random shaped particle. The technology makes it possible not only to directly characterize 3D morphology indices but also to investigate the aforementioned variations of 2D morphology indices with a relatively large number of 2D particle images. Therefore, with the utility of the 3D scanning technology, this research characterizes the variations in the 2D morphology values produced by different indices and projection angles at which 2D images are taken. Subsequently, the propagation of the variability to "Regularity" is further explored.

Wadell [26] proposed "true sphericity,  $\Psi$ ," as expressed by:

$$\Psi = \frac{S_{eq}}{S_a} \quad (1)$$

where  $S_a$  is the actual surface area of a particle and  $S_{eq}$  is the surface area of a sphere having an identical volume to the particle. While "true sphericity" requires measuring the volume and surface area of a particle, he also proposed "degree of sphericity [1]" (also referred to as diameter sphericity; herein denoted by  $S_D$  in Appendix A) that can be calculated from 2D images. Wadell also supplemented with elaboration of the detailed procedure of tapping the slide carrying the particle to sit on the largest plane face. Similarly, Wadell's roundness can be computed from the 2D image, particularly suggesting the projection angle that creates the plane by maximum and intermediate lengths. Krumbein [2]

\* Corresponding author.

E-mail addresses: [changhoon.lee@wne.edu](mailto:changhoon.lee@wne.edu) (C.H. Lee), [sjlee@fiu.edu](mailto:sjlee@fiu.edu) (S.J. Lee), [moochul.shfin@wne.edu](mailto:moochul.shfin@wne.edu) (M. Shfin).

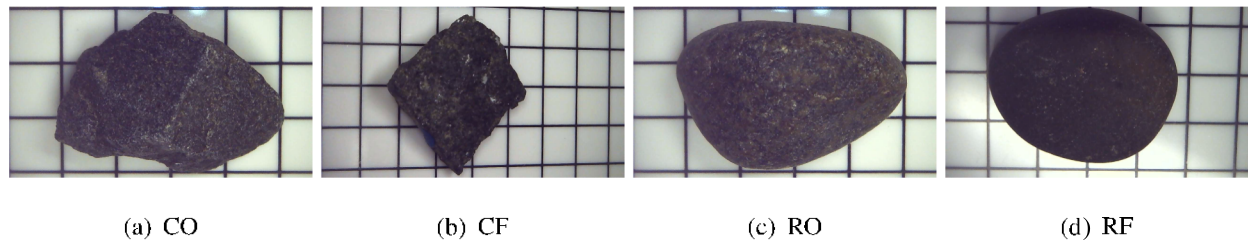


Fig. 1. Particles (Note that the grid size on the background is 5 mm).

Table 1

Descriptive Statistics of Morphology Indices ( $L$ ,  $I$ , and  $S$  respectively indicate the longest, intermediate, and the shortest lengths of a bounding box that encompasses the model with its minimum volume).

| ID | Number of Elements | Surface Area (mm <sup>2</sup> ) | $L$ (mm) | $I$ (mm) | $S$ (mm) | Wadefill True Sphericity ( $\Psi$ ) | Surface Area/element (μm <sup>2</sup> /element) |
|----|--------------------|---------------------------------|----------|----------|----------|-------------------------------------|---|
| CO | 13,697,779         | 705.66                          | 20.58    | 15.13    | 13.23    | 0.78                                | 51.52   |
| CF | 7,692,017          | 561.28                          | 19.05    | 18.82    | 5.17     | 0.60                                | 72.97   |
| RO | 9,078,249          | 715.69                          | 20.38    | 14.49    | 10.37    | 0.87                                | 78.84   |
| RF | 7,053,045          | 616.33                          | 18.38    | 15.74    | 7.04     | 0.82                                | 87.38   |

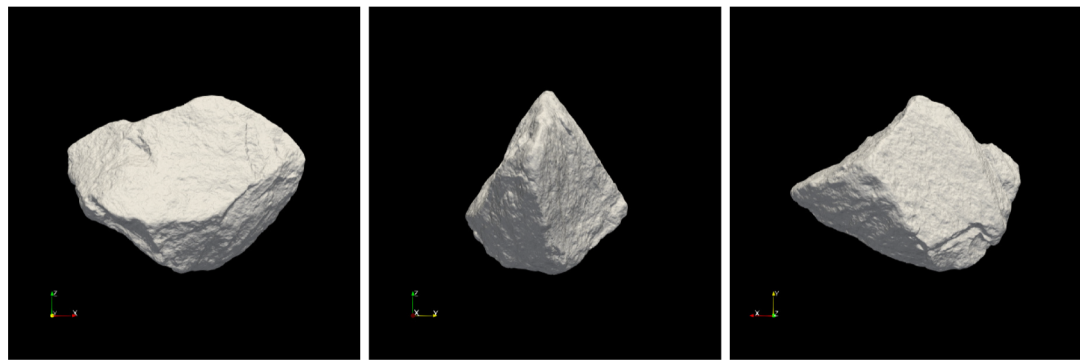


Fig. 2. Multiple projection views of Particle CO.

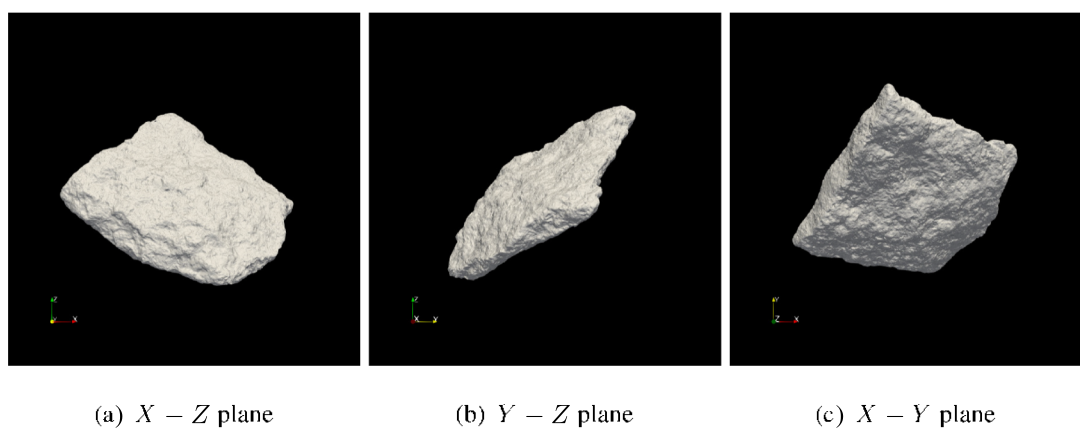


Fig. 3. Multiple projection views of Particle CF.

measured the roundness based on the largest projection image of a pebble to compare the resulting value with Wadefill's. However, the choice of the maximum projection angle was not necessarily required as implied by his comment, "There can be no objection to any other orientation [projection angle] if one wishes to use it, except that the values in that case cannot be directly compared with Wadefill's values

[2]." Nevertheless, Sneed and Folk [27] proposed the use of maximum projection area, proposing another sphericity index, "maximum projection sphericity," because the settlement velocity of a particle in the water is dominantly influenced by the area perpendicular to the direction of motion as referenced to Krumbein's experiment. As advanced numerical techniques such as meshfree learning algorithms have been

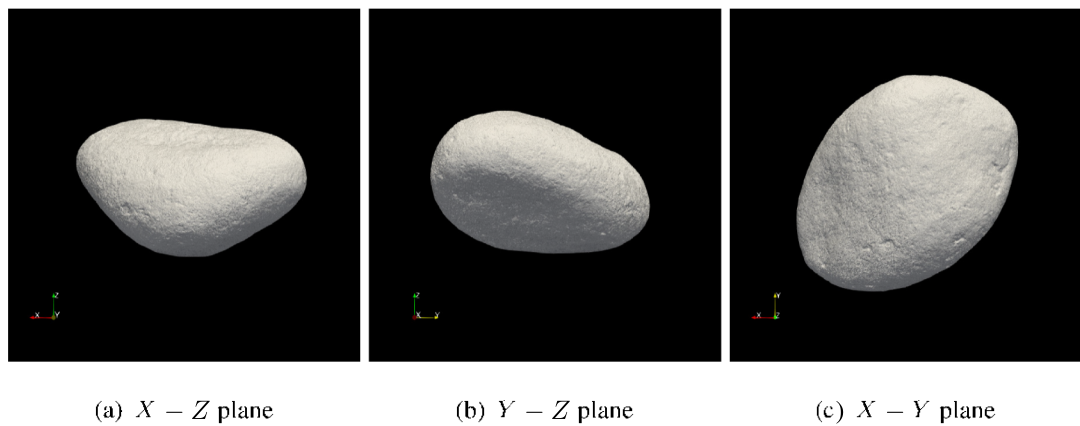


Fig. 4. Multiple projection views of Particle RO.

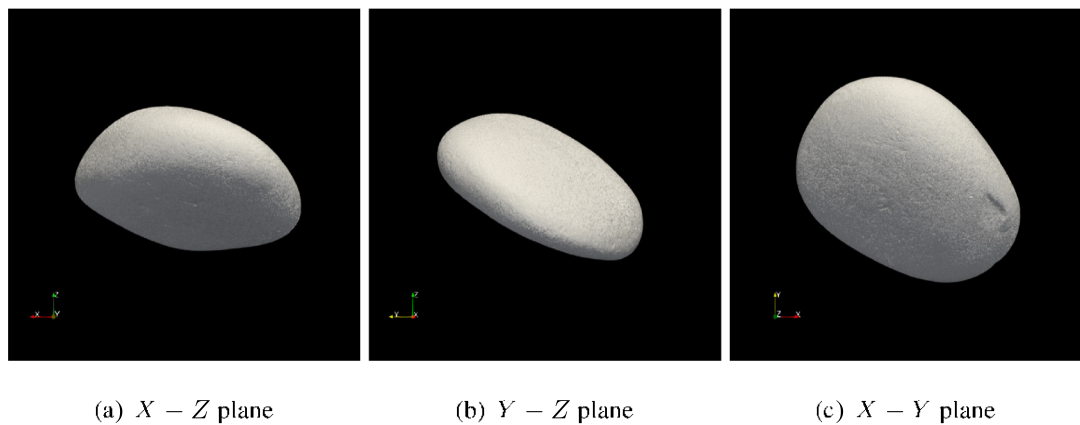


Fig. 5. Multiple projection views of Particle RF.

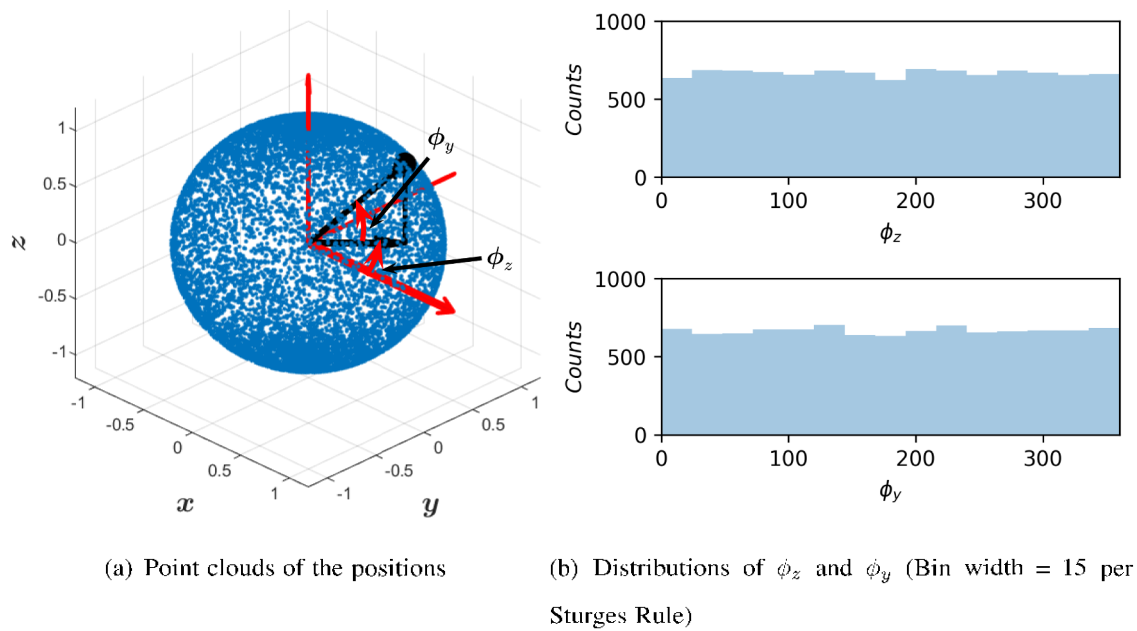


Fig. 6. Illustration of 10,000 randomly drawn camera positions.

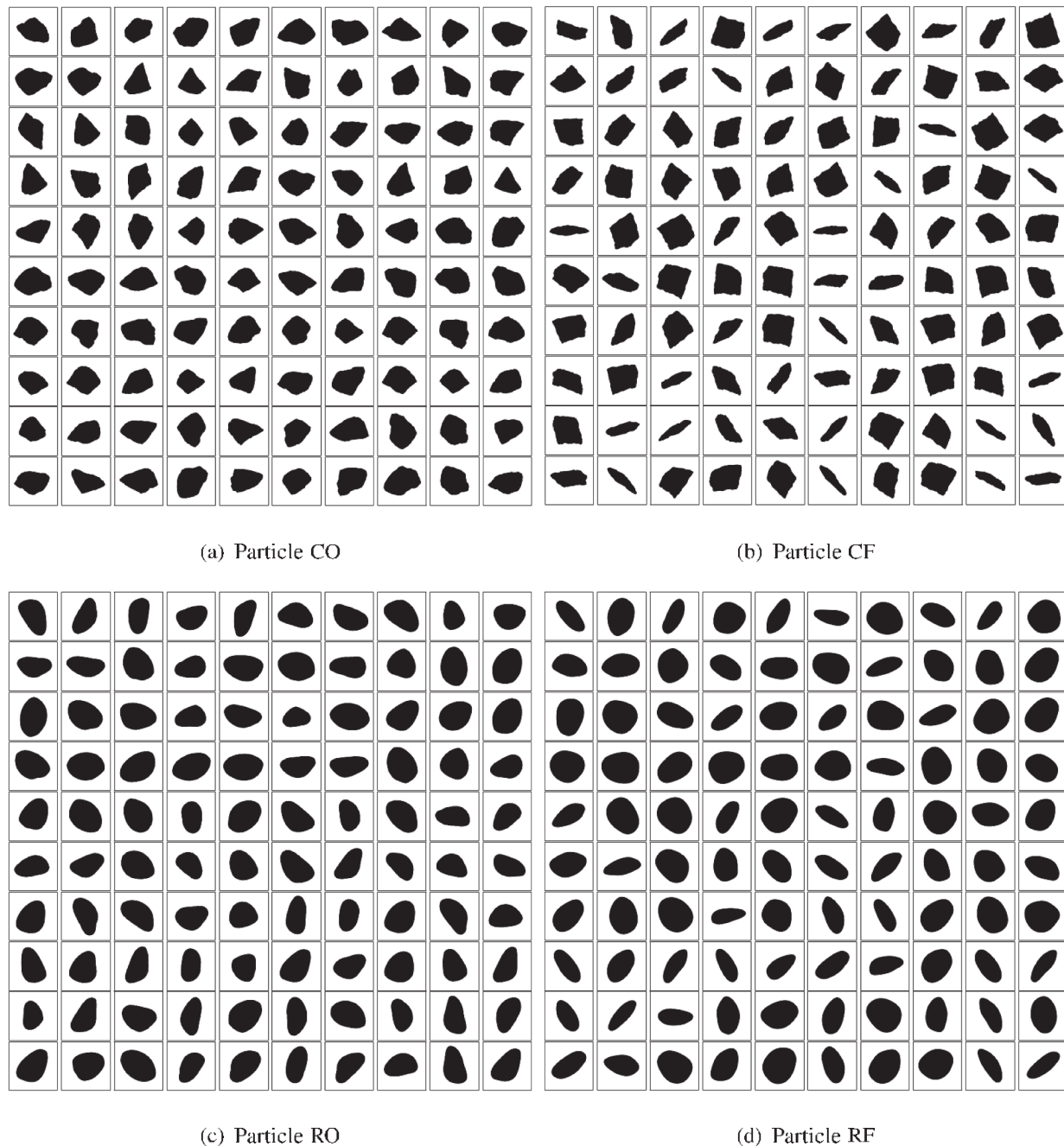


Fig. 7. 100 Image Samples for the Particles (Note that the images are displayed as  $10 \times 10$  array for each particle).

incorporated into the characterization of particle morphology, several researchers proposed methods to characterize morphologies of bulk particles [28–33]. These techniques are beneficial when aggregates are densely packed or stockpiled (e.g., riprap), enabling one to save labor and time in analysis of the bulk particle shapes, as opposed to a per-particle (single-particle) analysis; however, the morphology of each particle, particularly the effect of projection angles, would not be accurately considered in the "bulk view" analysis. Some researchers studied the effects of selecting projection angles on the computation of morphology indices. Wang et al. [34] reported that the difference of particle profiles characterized by Fourier analysis depending on variable orientations is statistically insignificant based on the images from three perpendicular projection angles, and it agrees with Su and Yan [35]'s conclusion from the investigation on 2D descriptors (Note that  $S_p$  and  $S_{WL}$  in Appendix A are commonly used for this research.). However,

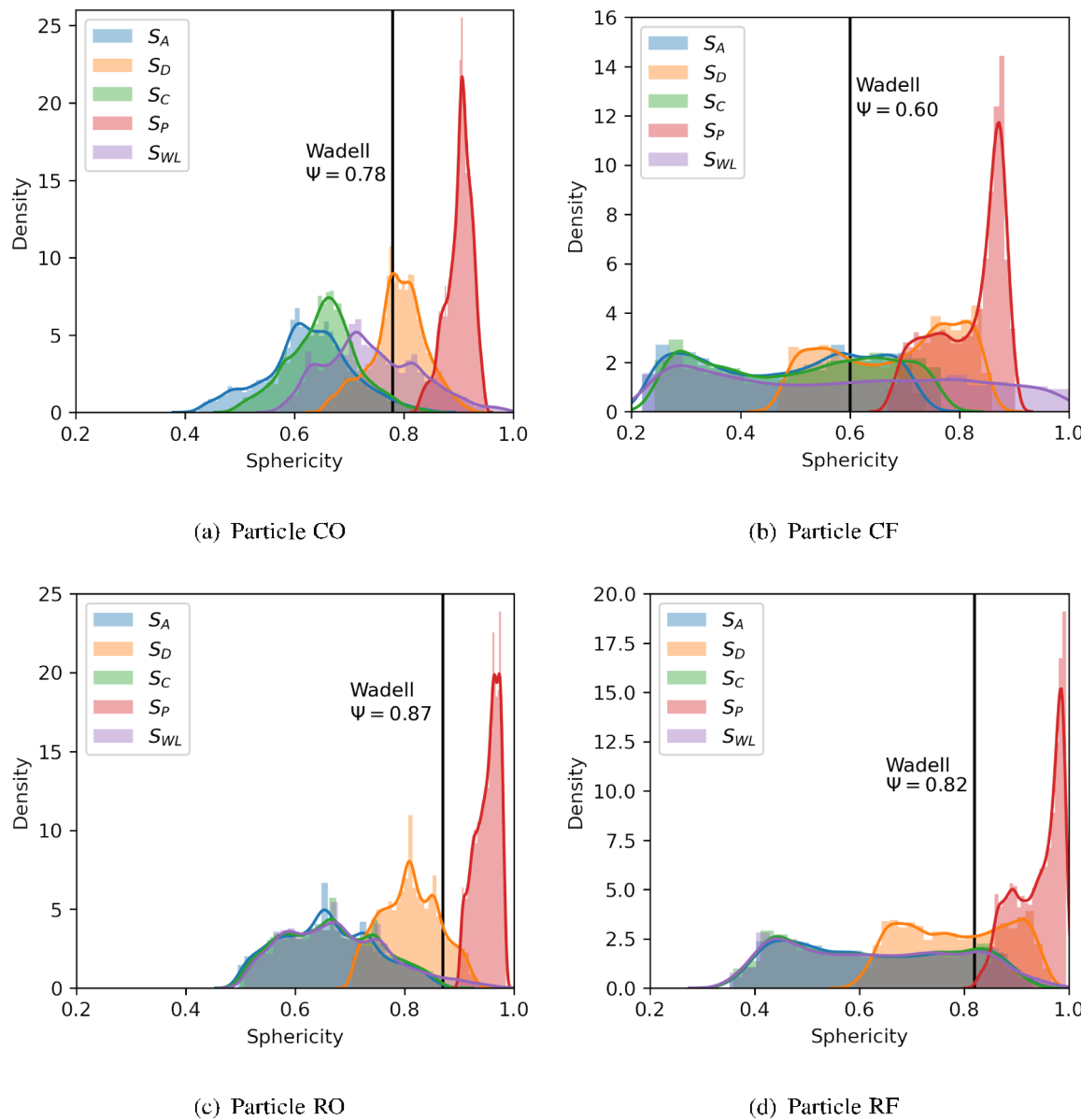
Maroof et al. [36] commented on a possible bias of the morphology indices because of orientations without any further systematic analysis.

As related to the projection angles (or orientation), the number of images for obtaining the reliable 2D morphology indices is also an interesting question. Wadeffl [26] commented "Strictly speaking, the total roundness of a soil is achieved by measurements in three planes at right angles to each other, but two planes are in most cases sufficient, while one plane is satisfactory when dealing with small sedimentary particles," implying that one or two 2D images would be sufficient in the computation of roundness. There is a lack of research on a sufficient number of images to reliably characterize the morphology of a single particle. Instead, several literature report the number of particles (in an image) for characterizing the morphology indices representing bulk particles. For example, Wang et al. [34] reported that 20 particles are enough to obtain statistically meaningful values. Zheng and Hryciw [30]

**Table 2**

Descriptive Statistics of Morphology Indices (Note that "PA" stands for "pixel area," defining the number of pixels for each particle image.)

| ID | Statistics | PA     | PCD   | RD    | $S_A$ | $S_D$ | $S_C$ | $S_P$ | $S_{WL}$ |
|----|------------|--------|-------|-------|-------|-------|-------|-------|----------|
| CO | $\mu$      | 707545 | 1204  | 0.431 | 0.626 | 0.790 | 0.653 | 0.901 | 0.743    |
|    | $\sigma$   | 101200 | 118.1 | 0.070 | 0.079 | 0.050 | 0.063 | 0.024 | 0.085    |
|    | CV         | 0.143  | 0.098 | 0.162 | 0.126 | 0.064 | 0.096 | 0.026 | 0.115    |
| CF | $\mu$      | 645497 | 1309  | 0.446 | 0.477 | 0.682 | 0.503 | 0.818 | 0.576    |
|    | $\sigma$   | 221213 | 60.2  | 0.069 | 0.152 | 0.113 | 0.158 | 0.063 | 0.229    |
|    | CV         | 0.343  | 0.046 | 0.154 | 0.318 | 0.166 | 0.314 | 0.077 | 0.398    |
| RO | $\mu$      | 804276 | 1249  | 0.777 | 0.659 | 0.810 | 0.666 | 0.951 | 0.676    |
|    | $\sigma$   | 129992 | 119.0 | 0.062 | 0.086 | 0.053 | 0.088 | 0.021 | 0.096    |
|    | CV         | 0.162  | 0.095 | 0.079 | 0.131 | 0.065 | 0.132 | 0.023 | 0.142    |
| RF | $\mu$      | 813270 | 1282  | 0.738 | 0.630 | 0.787 | 0.628 | 0.940 | 0.630    |
|    | $\sigma$   | 211827 | 62.0  | 0.138 | 0.157 | 0.099 | 0.157 | 0.045 | 0.161    |
|    | CV         | 0.260  | 0.048 | 0.187 | 0.249 | 0.126 | 0.250 | 0.048 | 0.256    |

**Fig. 8.** Histograms of Sphericities for Particles (Note that  $\psi$  is Wadell's true sphericity value).

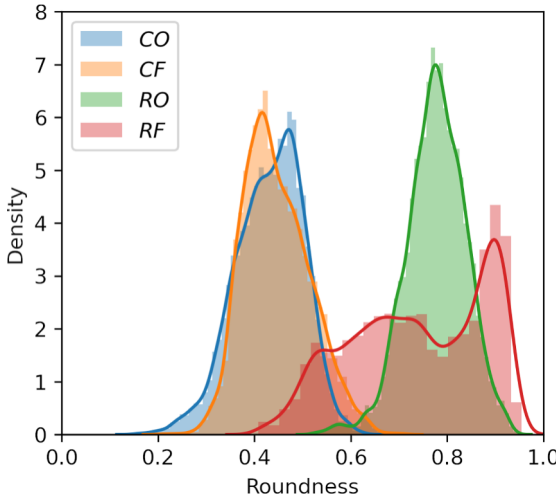


Fig. 9. Histograms of Roundness for Particles.

concluded that about 60 is required to achieve the value within 0.05 of the error at a 98% statistical confidence level, recommending to use 30–50 particles as a minimum. It is worthwhile to note that the investigation on the number of images (or particles) may be based on the rough assumption that a single value can represent the morphology of multifaceted, yet similar-shaped particles. However, it can potentially cause biases of the 2D morphology indices by ignoring their variations due to the orientations of individual particles.

Besides, another concern is whether a variety of 2D morphology indices can reasonably capture the 3D shape of a particle. Wadeffl [1,26,37] proposed “true sphericity” and roundness for correlating the particle shapes with the settlement velocity as done by other researchers [2,12,27]. However, as its application expands to various areas [38–40] beyond the subjects of geology, numerous efforts to solely characterize the 3D shape of particles have been proposed on the basis of various materials including random shaped particles [10,11,32,41–44]. Then, the concept of regularity is further introduced as combining [45,46] morphology indices at a different length scale with an aim of correlating with macroscopic behavior of the system. Furthermore, Wadeffl’s “true sphericity,” as expressed in Eq.(1), has been widely used as a reference for the comparison of various morphology indices. The name “true sphericity” might be a bit misleading because it is not only an indicator of the particle elongation but also the particle angularity. The “true sphericity” is a function of surface area, thus influenced by both elongation and angularity, and therefore has a concept of regularity that combines the overall morphology at different length scales. Nevertheless, Wadeffl [1] alternatively proposed a 2D sphericity index, herein  $S_d$ , as well as the “true sphericity,” he reported that the 2D index is generally comparable to the 3D  $\Psi$ -values as demonstrated by theoretical solids including sphere, cube, and three different parallelepipedes in the original paper. However, there is a lack of research exploring whether various 2D sphericities likely produce the similar value with “true sphericity.” Note that “true sphericity” is one of 3D morphology descriptors among others [27,41,42]. However, this study chose “true sphericity” as the reference sphericity index for evaluating 2D sphericity indices to examine if a good comparison can be made between 2D and 3D sphericities as Wadeffl has demonstrated for theoretical solids.

Accordingly, this research adopts the Monte-Carlo simulation approach [47] for characterizing the uncertainties of sphericities, exploring their propagation to the generalized regularity [46]. The associated analysis will demonstrate potential biases produced by 2D digital image processing when characterizing the morphology of particles. The results can provide possible challenges of a 2D image analysis due to the innate variability. The five different 2D sphericity and roundness indices, as summarized in Appendix A, are examined in this

study, and the following section will discuss the data acquisition procedure for obtaining a high-resolution 3D scanned model of a set of different particles and the Monte-Carlo simulation approach for further analysis. Lastly, the resulting variability of morphology indices, its propagation to the generalized regularity, and comparison of the values with “true sphericity” will be discussed.

## 2. Generation of 2D images from random orientations

### 2.1. Selection of particles

For a near equidimensional particle (e.g., sphere, cube, dodecahedron-like shape), the lesser variability in the sphericity can be expected. In other words, the variability due to projection angles becomes higher when the particle shape is “elongated” and/or “flat.” In addition, the particle’s angularity also changes depending on the projection angles at which the image is taken. For example, the roundness that measures the particle’s corner sharpness is evaluated with reference to the radius of maximum inscribed circle which may change depending on the projected angle. To characterize such variability of sphericity and roundness indices, four particles having significantly different shapes but similar maximum dimensional lengths (i.e., 18 to 20 mm) are selected as shown in Fig. 1. However, it is worthwhile to note that the selection of particles in this research targeted at demonstrating a bias of the resulting morphology indices produced by the variance by projection angles of the images.

The particles can be firstly grouped by two categories, “crushed (C)” and “riven (R)” particles, of which origins are significantly different; C-group is more angular than R-group by nature. Second, the particles are selected based on their ratios of lengths: “flat (F)” and “ordinary (O).” Herein, “F” is defined when the ratio of the intermediate length to the smallest length in a bounding box is greater than 2, otherwise the second nomenclature of the particle name is denoted by “O.” (The terms are referred according to ASTM C4791 [48].) For instance, the “CF” particle indicates a crushed particle with a flat shape.

### 2.2. Acquisition of 3D particle model

The 3D particle model is obtained by using a commercial Polylas C504 structured light 3D scanner [49], which output is either a wave-front (OBJ) or a stereolithography (STL) format file. Structured light scanner performs 3D scanning at 1:1 scale, thus the obtained 3D model has the actual particle size. The obtained 3D model is composed of 7 to 14 million triangular surface meshes, covering approximately 52–87  $\mu\text{m}^2$  per triangular mesh element for the considered particles. Table 1 summarizes the number of elements of each particle model, geometrical properties evaluated from the particle models, the corresponding  $\Psi$ , and the surface area/mesh density (Note that the specified accuracy of the scanner by the manufacturer is 6 microns).

Fig. 2–5 display 3D model images of each scanned particles on three orthogonal ( $x$ ,  $y$ ,  $z$ , and  $x$ ,  $y$ ) planes of the bounding boxes. On the authors’ opinions, the surface roughness is visibly well identified by the 3D images although the associated characterization is beyond the scope of this research.

### 2.3. Acquisition of 2D particle images from random orientation

A set of 2D images are obtained from each 3D particle model at 10,000 projection angles which are randomly selected from two independent uniform distributions of the rotational angles about  $z$ - and  $y$ -axes, denoted by  $\phi_z$  and  $\phi_y$ , respectively. (i.e.,  $\phi_z \in [0, 360]$  and  $\phi_y \in [0, 360]$ ). Fig. 6 (a) shows the camera positions, which identified and applied to all four particles, and Fig. 6 (b) displays the distributions of  $\phi_z$  and  $\phi_y$ . Note that the sample size of 10,000 adopted in this study has been widely used for the Monte Carlo simulation [50,51], and the

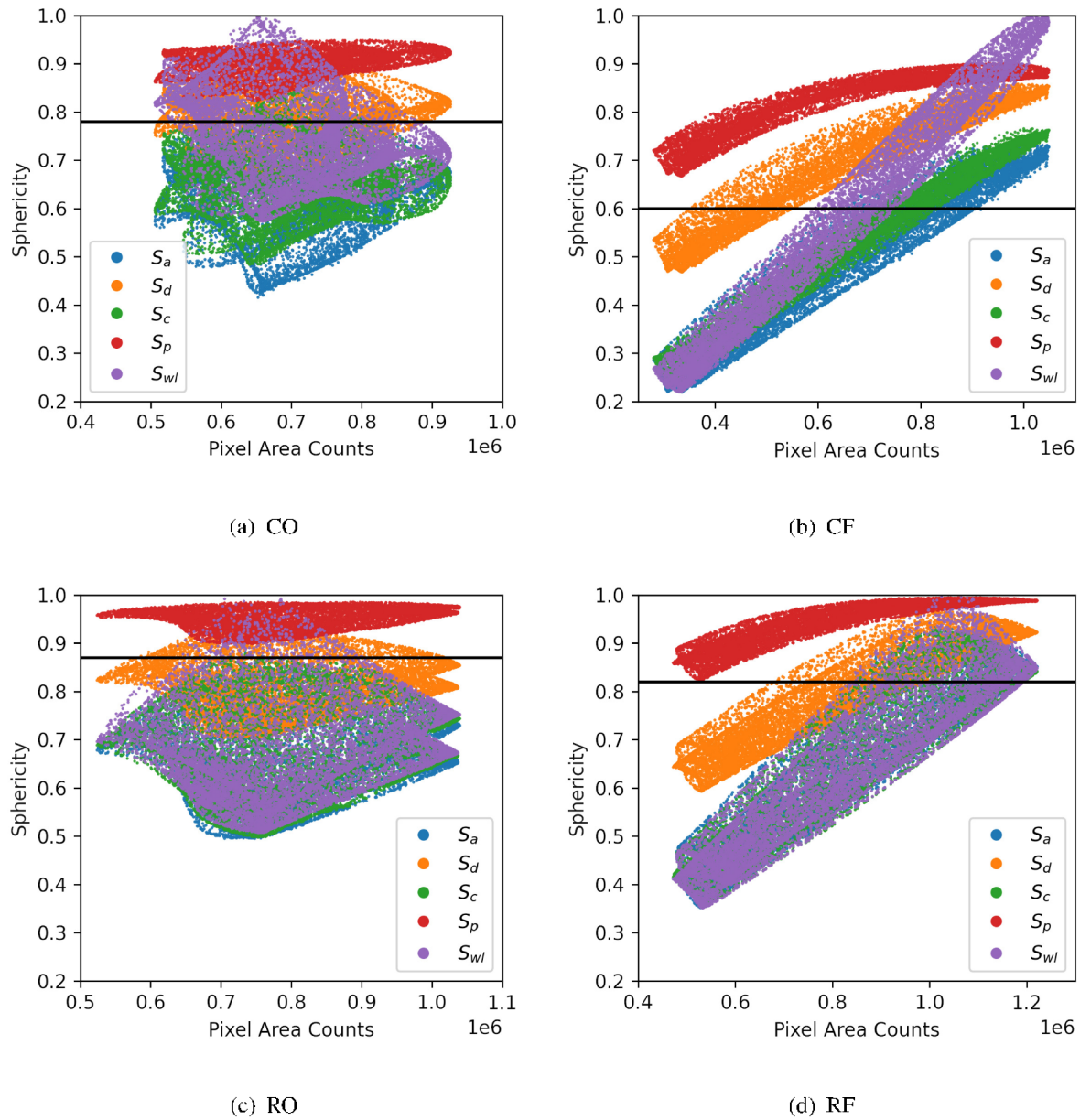


**Fig. 10.** Sphericity with Pixel Area (Note that the black line indicates Wade's "true sphericity").

combination of  $\phi_z$  and  $\phi_y$  is not sampled from the structured grid on a virtual globe encompassing the particle. However, the number of samples can be set such that each view is approximately taken every 3.6° of  $\phi_z$  and  $\phi_y$ .

Fig. 7 shows 100 sample images of each particle. It is worth while to note that Wade [1,26] mentioned that the largest dimensional length must be set to be about 70 mm regardless of pebbles or sands for which scaling of the image is necessary. Equivalently, when using the image analysis technique, Zheng and Hryciw [52] suggested that each image must be taken to represent the circumferential circle diameter by more than 1000 pixels (i.e., 1000 pixels per circumference circle diameter (PCD)). Otherwise, the resolution of the image cannot effectively capture the small corners for the roundness calculation [30]. This study adopts about 1,200 of average number of pixels to properly capture the PCD according to the recommendation by Zheng and Hryciw [52], as summarized in Table 2.

#### 2.4. Computation of sphericity and roundness

The obtained 2D images are converted to a binary format for the computation of sphericity and roundness indices. This study adopted five commonly accepted sphericity indices ( $S_a$ ,  $S_d$ ,  $S_c$ ,  $S_p$ ,  $S_{wl}$ ) in the aggregate research community [46] as listed in Appendix A. All of the indices are designed to have a value between 0 and 1. The algorithm developed by Zheng and Hryciw [52] is used for the evaluation of the morphology indices (i.e. sphericity and roundness).

#### 3. Variation in sphericity and roundness indices

According to the aforementioned procedures, the values of morphology indices, five sphericities and a roundness, are computed. Table 2 summarizes the descriptive statistics of the computed five sphericities and roundness. Also, Figs. 8 and 9 show the kernel densities [53] of the roundness and sphericity values, respectively, for minimizing potential biases produced by the binwidth of histograms.

The different degrees of variance in the resulting sphericity and

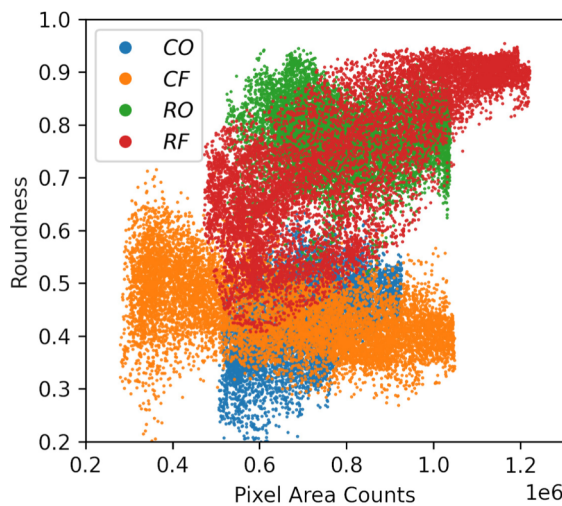


Fig. 11. Roundness with Pixel Area.

Table 3

Number (Percentage) of images that produce the 2D sphericity indices close to “true sphericity”.

| 2D Sphericity | CO          | CF          | RO          | RF          |
|---------------|-------------|-------------|-------------|-------------|
| $S_A$         | 75 (0.75%)  | 242 (2.42%) | 18 (0.18%)  | 211 (2.11%) |
| $S_D$         | 969 (9.69%) | 211 (2.11%) | 355 (3.55%) | 270 (2.70%) |
| $S_C$         | 106 (1.06%) | 199 (1.99%) | 19 (0.19%)  | 204 (2.04%) |
| $S_P$         | 0 (0.00%)   | 0 (0.00%)   | 0 (0.00%)   | 10 (0.10%)  |
| $S_{WL}$      | 304 (3.04%) | 127 (1.27%) | 64 (0.64%)  | 176 (1.76%) |

roundness indices are displayed in Figs. 8 and 9. It is observed that the computed sphericity and roundness values for a given particle are varied with respect to the definition of sphericity and the projection angles. The variations according to different sphericities are conceptual and procedural factors, while it can be said that those with respect to projection angles are engendered by intrinsic particle shape properties. Such variances are relatively larger for particles CF and RF particles with flat shapes; for example, the obtained values of  $S_{WL}$  range from 0.22 to 0.99 and 0.16 to 0.99 for CF and RF, respectively. Amongst the sphericity indices,  $S_p$  showed the smallest variance regardless of particles; however, the difference between the minimum and maximum values produced by the projection angles still ranges from 0.1 to 0.2 depending on the particles. In addition, it is observed that the density functions of  $S_A$ ,  $S_C$ , and  $S_{WL}$  for both RO and RF particles are similar. The result distribution of  $S_A$  shifted to left of the distribution of  $S_D$  because  $S_A \ll S_D$  by definition (i.e.,  $S_A = S_D^2$ ) (the proof of the relationship can be found in [46]). However, the standard deviation of  $S_A$  is accordingly larger than  $S_D$  regardless of particles as shown in Table 2, which is induced by differences in the definition of the sphericity.

In Fig. 8, the Wadeffl's “true sphericity” is also shown as a reference value. The true sphericity is a 3D shape index, and therefore, only one value is obtained per particle. Therefore, the comparison can be used to evaluate how close the computed 2D sphericities are to the “true sphericity.” Wadeffl [1] suggested a 2-D sphericity index, herein denoted by  $S_D$ , as demonstrating that the value is close to the true sphericity of a sphere, cube, and three different parallelepipeds. However, unlike the theoretical shapes, it is observed that the likelihood that  $S$  is identical to Wadeffl's “true sphericity” is low for mineral particles in nature. The associated details will be further discussed in Section 5.

Fig. 9 shows the kernel densities of the roundness. The mean values of roundness for RO and RF (rivar particles) are higher than those for CO and CF (crushed particles). The roundness of CO, CF, and RO are spread with an approximately  $\pm 0.2$  in the center of the means, while that of RF is wider ranging from 0.4 to 0.95. Besides, the density of roundness for RF

has two peaks observed at approximately 0.65 and 0.9, which could be an indication that a 2D roundness value can be misinterpreted when 2D images are obtained at certain projections angles and/or with limited numbers.

#### 4. Influence of projection area on variability of sphericity and roundness

The variance demonstrated in Figs. 8 and 9 excludes any effect produced by altering the projection angles. The views from different angles surely change morphology parameters, yet any dependency on the projection area is of interest in this section. Although Wadeffl and other researchers [1,2,26,27] recommended (or at least used for the comparison) the utility of the maximum projection angles, it is apparently expected that the morphology parameters could be changed, particularly considering a particle of which shape is flat such as a coin. Besides, some parameters (i.e., herein,  $S_A$ ,  $S_D$ , and  $S_p$ ) are a function of the projection area, while the other uses the properties of inscribing or circumscribing circles that are influenced by the area. Therefore, this section investigates the relevance of the projection area (by pixels) to the sphericity and roundness evaluation.

The sphericity and roundness with respect to the number of pixels representing a particle's projected area (so-called “pixel area”) are shown in Fig. 10 and Fig. 11, respectively. As the distance of a particle and camera is fixed, the number of pixels for the area can directly represent the projection area for the given particle. As observed in Fig. 10, the variance of the sphericity indices for the four selected particles is relatively smaller at the lower and higher projection areas, while the rate of variance changes with the pixel area depends on the particles and sphericity indices. However, the limited number of images (i.e., a portion of 10,000 images) obtained from those two extreme ends causes the smaller variation. In addition, from the analysis of four selected particles, all sphericities tend to increase with the number of pixel areas for the particles with flat shapes (Particle CF and RF). This attributed to the smaller area of CF and RF is equivalent to the elongated shape displayed in a given image. However, such an increase was not observed in ordinary particles (i.e., RO and CO). As will be discussed in Section 5, the resulting value does not necessarily correspond to the “true sphericity.”

It is worthwhile to note that Wadeffl [37] highlighted the importance of the maximum projection area for calculating the roundness because the size of the maximum inscribed circle depends on the projection angles. It is observed from Fig. 11 that the difference between the maximum and minimum roundness obtained on the maximum projection area is still approximately 0.2 (See at the right end of roundness point clouds in Fig. 11.) regardless of the particles while the overall variation is about 0.5. Fig. 9 shows two groups of the densities (i.e., CO/CF vs. RO/RF), indicating the roundness of “R” group is higher than that of “C” group (i.e., in the context of the mean values). When investigating the roundness values with respect to the size of the area, it is observed that roundness increases as the area increases for particles CO and RF and decreases for particle CF. Particle RO does not show a particular trend. Therefore, it concludes preliminarily that there is no clear relation of the projection area to the roundness unlike Wadeffl's conjecture on the projection area dependency [37].

#### 5. Comparison of 2D-sphericity with Wadeffl's true sphericity

True sphericity proposed by Wadeffl [26] is a function of the surface area and volume of a particle, as expressed in Eq.(1), and both variables must be measured in a 3D nature. The measurement of surface area is challenging, and therefore 2D sphericity indices were developed and have been widely used instead of the true sphericity. Even if some similarity between the true sphericity and 2D sphericities is generally implied as Wadeffl [1] reported, it is evidently observed from Fig. 8 that there is a small chance that 2D indices are close to the “true sphericity” even if the tolerance of  $\Psi \pm 0.025$  is considered (per Wadeffl estimation

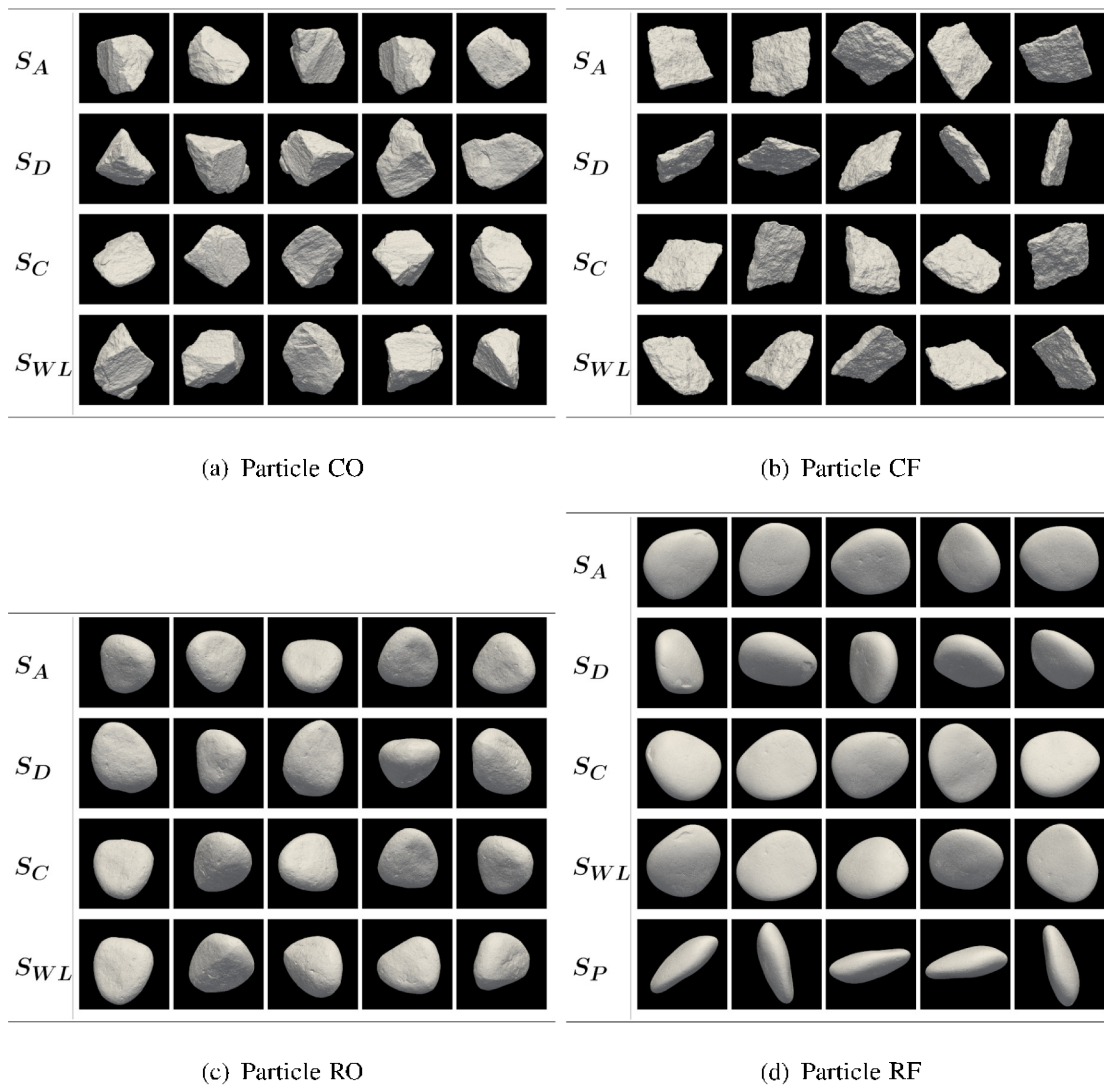


**Fig. 12.** Image Samples producing 2D Sphericities close to True Sphericity.

on the “error” of 2D sphericity index (i.e.,  $S_D$ ) [37]. Furthermore, Fig. 10 demonstrates that the maximum projection area of a given image does not guarantee that the computed 2D sphericity index is close to the aforementioned tolerance. Nevertheless, it is also true that some sphericity indices computed with the images at some particular angles can be close enough to be the true sphericity, thereby exploring any noticeable pattern on such images and/or angles. However, the extent of the observed difference may depend on the selection of particles, and the results are limited to the particles used for this research.

Table 3 summarizes the number of 2D images which yielded close to the “true sphericity” within the Wadeff’s tolerance (i.e.,  $\psi \pm 0.025$ ). Amongst 10,000 images for each particle, it is observed that the number of images satisfying the tolerance is from 0 to 969 images depending on the sphericity indices. Particle CO had the highest chance (i.e., 9.69%) of being close to the true sphericity value when using  $S_D$ , while there was none (i.e., 0%) when using  $S_P$  for CO, CF, and RO. If one chooses the use of  $S_P$ , the chance of obtaining a 2D index value close to the 3D index is up to around 2.5% for flat particles (i.e., CF and RF) and less than 1% for the ordinary shape of particles. A similar trend of particle dependency is observed in the case of  $S_C$ . On the other hand,  $S_WL$  shows a relatively greater chance of fitting the 3D value for CO. Therefore, except for the case of  $S_D$  computed from CO images, the percentage of obtaining 2D indices close to the 3D index approximately ranges up to 3% per our observation, translating to only 1 to 3 images out of 100 images. Fig. 12

shows five sample images per each sphericity index on which the sphericity value is close to the “true sphericity” within the tolerance. As previously mentioned, the images that can obtain maximum projection area doesn’t always provide the 2D indices close to the “true sphericity.”

Fig. 13 displays the kernel density of  $\phi_z$  and  $\phi_y$  that produces the 2D sphericity index close to the true sphericity. Among the number of images summarized in Table 3, the set of  $\phi_z$  and  $\phi_y$  in the relatively higher densities indicated by the lighter color is more likely to obtain the value close to “true sphericity.” Although no clear pattern is observed, one to three highest density regions are observed according to the sphericity index and the particles. For example, in case of CO- $S_A$  (Fig. 13 (a)), the angle of  $\phi_z$  is identified at about 125 degrees while the corresponding  $\phi_y$  is found at approximately 100 and 325 degrees, which indicates that both the projection views of the groups are symmetric about  $\phi_y = 225^\circ$ . For  $S_WL$  of RO, two highest density groups are observed at  $\phi_z = 150^\circ$ ,  $\phi_y = 90^\circ$  and  $\phi_z = 250^\circ$ ,  $\phi_y = 275^\circ$ . Two groups can be symmetric about  $\phi_z = 200^\circ$ ,  $\phi_y = 183^\circ$  (i.e., the opposite side in terms of  $\phi_y$ ), yet the angle does not provide the maximum projected area as seen from Fig. 12 (c). It is important to note that specific values of angles reported and/or discussed herein are limited only to the specific orientations and the particle models implemented in this research; and they will be

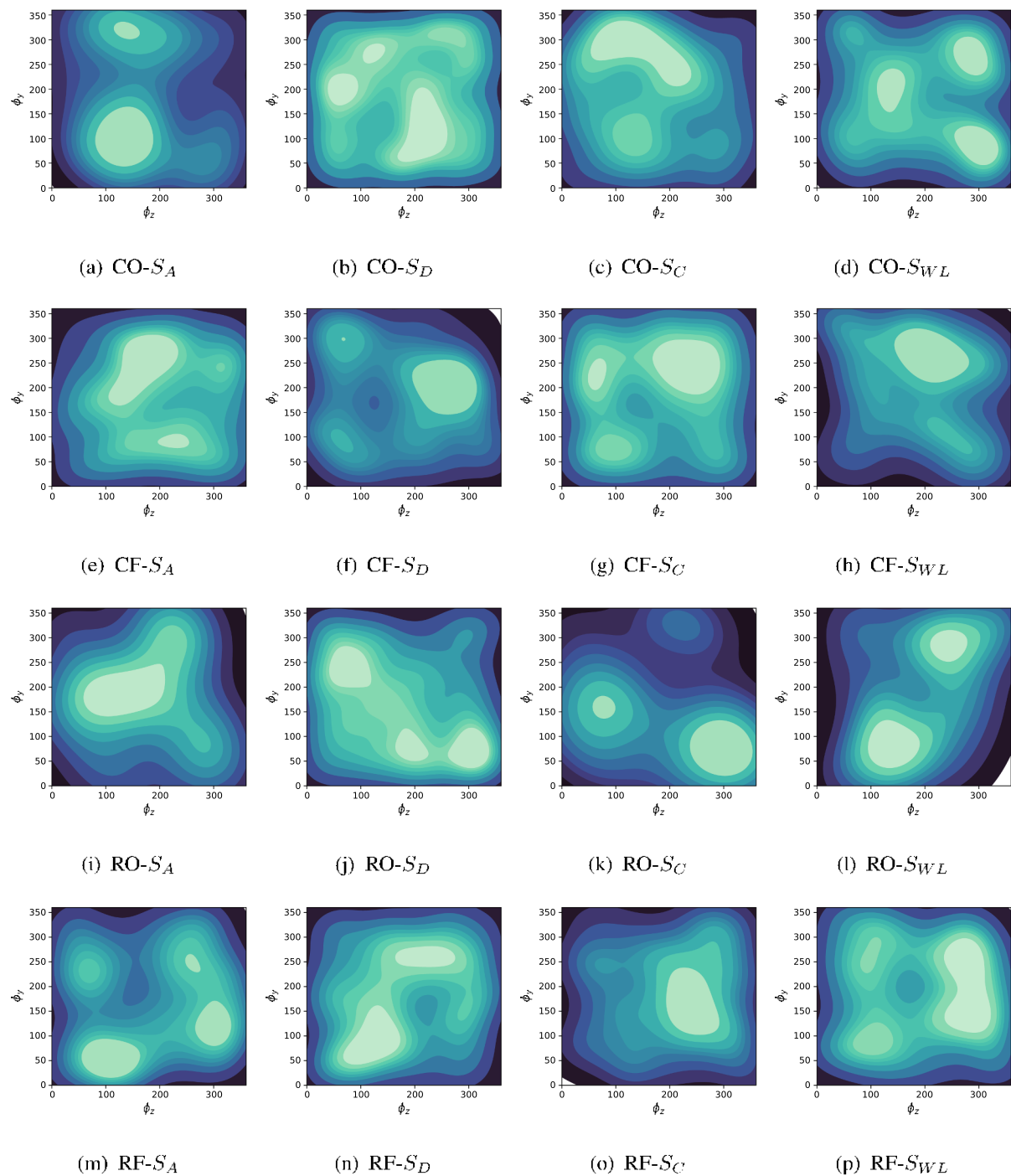


Fig. 13. Kernel Density Contour of  $\phi_z$  and  $\phi_y$  to produce 2D Sphericity close to "True Sphericity".

different according to the orientation of the implemented coordinate system and/or particle placement. Despite weakly discernible evidence, further research must be performed to quantify patterns. Although a sample size of 10,000 is used for the Monte-Carlo simulation in this research, only a limited number of images satisfy the threshold (i.e., the maximum of 9.69% in Table 3) in generating Fig. 13. Also, definitions of various 2D sphericities (at least used herein) may not effectively capture 3D information in "true sphericity," thereby requiring further studies.

## 6. Variability of regularity

The regularity is a parameter that combines sphericity and roundness together, having been used to correlate with mechanical and/or rheo-

logical behavior of a system of particles. While Cho et al. [45] proposed a regularity calculated by an arithmetic average of the sphericity and the roundness, Lee et al. [46] reported the sensitivity of the sphericity and the roundness for defining "weighted Regularity (or Angularity)" are different, suggesting a generalized regularity incorporated into Confirmatory Factor Analysis (CFA) [54,55]. The corresponding equation can be written as:

$$\text{Regularity} = (1 - \xi_i) \times \text{Sphericity} + \xi_i \times \text{Roundness} \quad (2)$$

where  $\xi_i$  (0 ≤  $\xi_i$  ≤ 1) is a weight coefficient (Note:  $\xi_1 = 1$  ( $S_1$ ),  $\xi_2 = 2$  ( $S_2$ ),  $\xi_3 = 3$  ( $S_3$ ),  $\xi_4 = 4$  ( $S_4$ )) [46].

Usefulness of a regularity is still controversial [45,46,56]; an

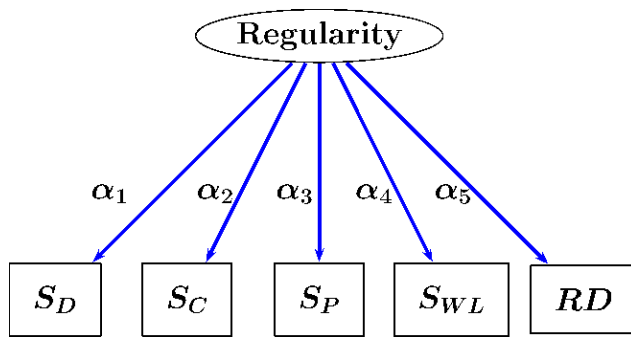


Fig. 14. Confirmatory Factor Analysis Model.

Table 4  
The factors from CFA Analysis.

| CFA Coefficients              | CO    | CF    | RO    | RF    |
|-------------------------------|-------|-------|-------|-------|
| $S_D (\alpha_1)$              | 1.000 | 1.000 | 1.000 | 1.000 |
| $S_C (\alpha_2)$              | 1.261 | 1.369 | 1.675 | 1.575 |
| $S_P (\alpha_3)$              | 0.435 | 0.505 | 0.386 | 0.437 |
| $S_{WL} (\alpha_4)$           | 1.527 | 1.928 | 1.820 | 1.627 |
| $RD (\alpha_5)$               | 0.018 | 0.274 | 0.275 | 1.148 |
| CFI                           | 0.99  | 0.99  | 0.95  | 0.92  |
| $\xi_i$ from CFA coefficients |       |       |       |       |
| $\xi_1$ (by $S_D$ )           | 0.982 | 0.785 | 0.784 | 0.466 |
| $\xi_2$ (by $S_C$ )           | 0.986 | 0.833 | 0.859 | 0.578 |
| $\xi_3$ (by $S_P$ )           | 0.960 | 0.648 | 0.584 | 0.276 |
| $\xi_4$ (by $S_{WL}$ )        | 0.988 | 0.876 | 0.869 | 0.586 |

approach of using a single parameter instead of two is simpler when correlating the morphological findings with macroscopic behaviors, while it can be argued that the Regularity may not effectively capture the change of individual morphology at different length scales (i.e., elongation and angularity). While demonstrating the efficacy of the Regularity is beyond the scope of this research, this section focuses investigating the variability of the resulting Regularity engendered by projection angles.

From the CFA model shown in Fig. 14, the analysis determines the coefficients (i.e.,  $\alpha_1$  to  $\alpha_5$ ), indicating the change of the sphericity and roundness values according to the unit change of the construct, "regularity." Note that  $S_A$  is excluded from the model because of  $S_A = S_D^2$  [46]. Since  $\alpha_1$  is set to 1.0, as shown in Table 4, the coefficients can be used for quantifying the relative sensitivity of the coefficients (i.e.,  $\alpha_1$  to  $\alpha_5$ ). It is noted that the change of regularity in this research is caused by different projection angles. Thus, when the projection angle changes, the CFA coefficients represent how much sphericity and roundness relatively change as compared to  $S_D$ . Accordingly, the results compare the relative sensitivity amongst the different sphericity findings for defining "Regularity," further computing the weight factors ( $\xi_i$  in Eq. (2)) as maximizing the discrimination. The open-source R-package [57] for the structural equation modeling, "lavaan [58]," is used, and the results of CFA on the model are summarized in Table 4. The resulting values of CFI (Comparative Fit Index) (i.e.,  $> 0.9$  regardless of particles) reveals that the coefficients are statistically significant [54,59]. Negative CFA coefficients of the roundness for CO and CF are obtained, translating that the increase of regularity causes to decrease the roundness. The weight factor,  $\xi_i$ , is computed for calculating the Regularity. (Note that the details of the computational method are described in B.)

Based on the weight factors, the generalized regularity is computed as shown in Fig. 15. Fig. 15 (a) shows that the difference in the density functions on the basis of different sphericity findings for CO particle is negligible. This is attributed to the fact that  $\xi_1$  is greater than 0.96, inferring that the more than 96% regularity is determined by the value

of roundness. Thus, the difference in the values of sphericity practically ineffective when it comes to the computation of "weighted" regularity. The variance in the regularity is largest for RF particle, and it is manifested by relatively smaller values of  $\xi$  in the numerical sense. Thus, the bimodal pattern of the sphericity findings become more discernible in the regularity, and the higher value of the regularity is obtained by the larger projection area as shown in Fig. 10. For particles CF and RO, the regularity densities calculated by  $\xi_2$  (by  $S_C$ ) and  $\xi_4$  ( $S_{WL}$ ) are similar because the corresponding CFA coefficients show similar sensitivities according to the change of the construct, Regularity.

The variance of the generalized regularity can be propagated from those of individual sphericities and the roundness depending on the values of their variances, covariances, and coefficients  $\xi$ . Accordingly, the resulting variance of the regularity computed from the four selected particles herein can either increases or decreases. From the results, it is observed that the variance of the regularity for the CF particle significantly decreases, while no further propagation of uncertainties is observed in other particles.

## 7. Concluding remarks

This study investigates the uncertainties in 2D sphericity and roundness produced associated with the projection angles and their propagation to the generalized "weighted" regularity. This research selected four particles to demonstrate a potential bias of the resulting value of morphology findings. Based on the results, the following conclusions are drawn:

- (1) The variability of sphericity and roundness produced by images taken from 10,000 projection angles is significant, and its extent depends on its definition and origin. The variance of sphericities increases when the particle is flat. While Wadeffl [37] reported the difference of 0.05 in the sphericity can classify a given particle shape differently (i.e., error tolerance of computation), the resulting variability obtained from research is large enough to mislead the particle shape. Such a large variation is also observed in the roundness.
- (2) Such variations in sphericities and roundness are propagated to the computation of "weighted regularity." However, the variations of the regularity depend not only on the definitions of sphericity but the sensitivity of sphericity and roundness for defining "Regularity" influences the variation. Nevertheless, no significant propagation of the variation is observed except for CF particle that the variance decreased.
- (3) Although the use of the maximum projection angle is suggested by early researchers [2,26,27], its practicality in the current practice may not be highlighted, particularly in the acquisition of shape findings for bulk aggregates. However, it is observed that the variance relatively decreases when taking the maximum projection area. Nonetheless, the 2D sphericity values are not necessarily close to the "true sphericity" proposed by Wadeffl [37].
- (4) Instead of using maximum area projection angle, this study investigates a pattern of projection angles that produces the 2D sphericity values close to the "true sphericity," although its quantification remains for the future study.
- (5) With recent advances in 3D scanning technology, high-resolution 3D shape imaging is getting more feasible with reduced amount of time and cost. Therefore, further study needs to be made in the research community for wider use of 3D findings and standardization of the process as the 3D morphology index accurately represents the particle geometry compared to the conventional 2D morphology findings that produce a large variance in the results depending on how images are obtained.
- (6) While significant variances from the projection angles are observed for the carefully selected four particles with different geometries, the extent of variances in the 2D sphericity and roundness findings may depend on the characteristics of particles (e.g.,

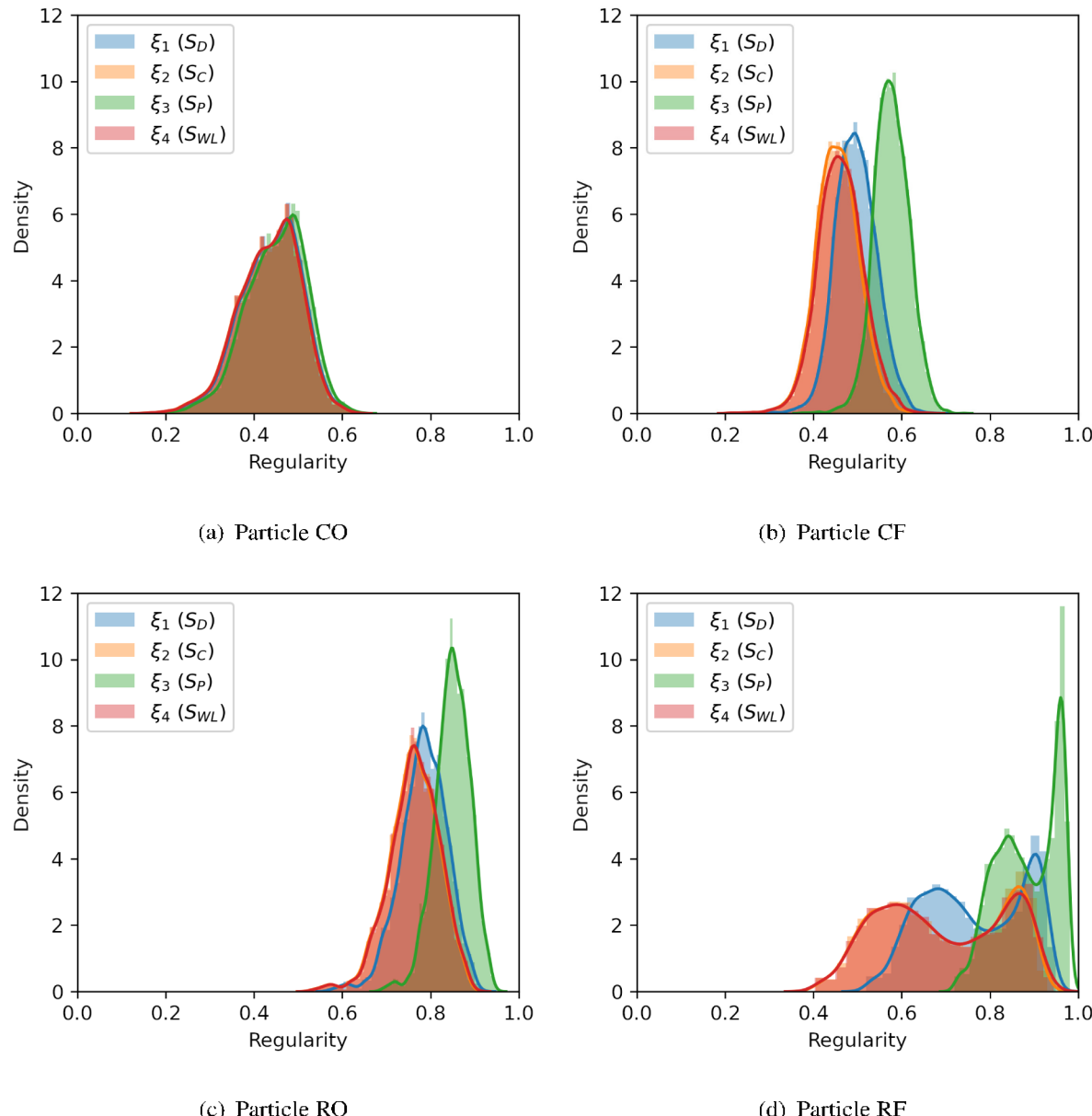


Fig. 15. Histograms of Regularity.

concavity, source) and the implemented digital imaging process (e.g., method, resolution, tolerance of the analysis). Therefore, further research is recommended on this topic for more parametric studies.

#### Declaration of Competing Interest

The authors declare that they have no known competing financial interests or personal relationships that could have appeared to influence the work reported in this paper.

#### Appendix A. Sphericity and roundness indices

The sphericities and roundness implemented for this study (adapted from [52]) are summarized below. Fig. A.16 depicts the variables required for computing sphericities and a roundness.

$$\text{Area sphericity : } S_A = \frac{A_s}{A_{cir}} \quad (\text{A.1})$$

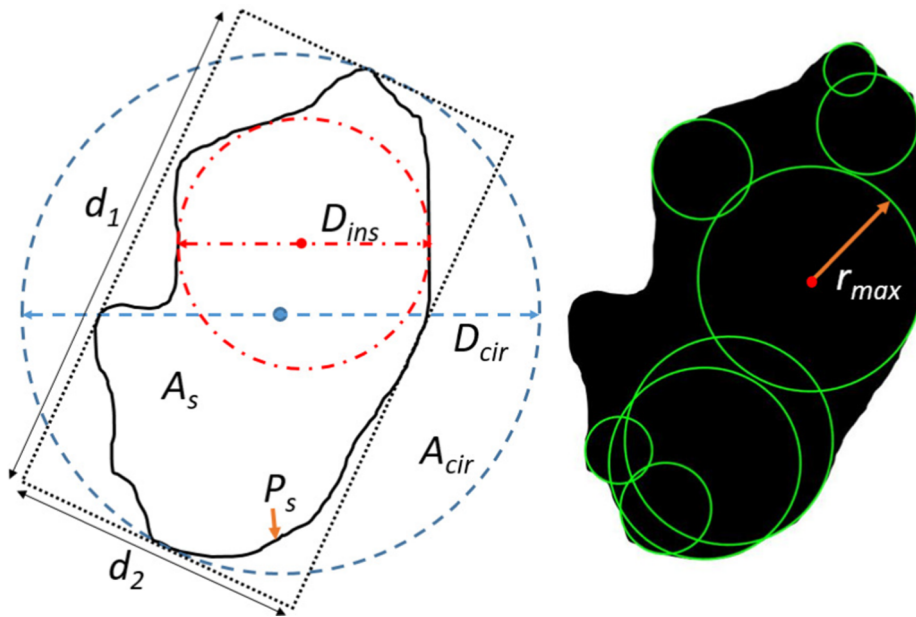


Fig. A.16. Schematic of variables for computing sphericities and the roundness.

$$\text{Diameter sphericity : } S_D = \frac{D_c}{D_{cir}} \quad (\text{A.2})$$

$$\text{Circle ratio sphericity : } S_C = \frac{D_{ins}}{D_{cir}} \quad (\text{A.3})$$

$$\text{Perimeter sphericity : } S_P = \frac{P_c}{P_s} \quad (\text{A.4})$$

$$\text{Width to length ratio sphericity : } S_{WL} = \frac{d_2}{d_1} \quad (\text{A.5})$$

$$\text{Roundness : } RD = \frac{\sum_i (r_i/r_{max})}{N} \quad (\text{A.6})$$

where:

|             |   |
|-------------|---|
| $A_s$ =     | Projection area of a 2-D particle image   |
| $A_{fir}$ = | Area of the minimum circumscribing circle enveloping a projected particle image                   |
| $D_c$ =     | Diameter of a circle with the same projected area as a given particle                             |
| $D_{fir}$ = | Diameter of the minimum circumscribing circle enveloping a projected particle image               |
| $D_{ins}$ = | Diameter of the maximum inscribing circle   |
| $P_c$ =     | Perimeter of a circle with the identical projected area as a particle ( $= \sqrt{\pi A_s}$ )      |
| $P_s$ =     | Perimeter of the 2-D particle image   |
| $d_1$ =     | The largest dimension length of a given particle (orthogonal to the direction $d_2$ is measured.) |
| $d_2$ =     | The width of a given particle (orthogonal to the direction $d_1$ )                                |
| $\eta_i$ =  | Radius of curvature of the corner of green circles fitted to corners in Fig. A.16                 |
| $r_{max}$ = | Radius of the maximum inscribed circle (radius of the largest green circle in Fig. A.16)          |

## Appendix B. Derivation of weight coefficient for generalized regularity

Supposed that the estimated parameters from CFA for two indicators are denoted by  $\alpha_i$  and  $\alpha_j$ . Fig. B.17 illustrates the magnitudes of the parameters by the length of diameter. Therefore, the weight coefficients ( $\xi$ ) in Eq.(2) can be represented by the distances from the center of two circles, and the regularity of Eq.(2) can be represented by the black solid point marked as "weighted average".

The weighted average of two factors (i.e., first moment in the statistics) is expressed by:

$$|\alpha_i|\xi_i = |\alpha_j|\xi_j = m \quad (\text{A.7})$$

$$\xi_i + \xi_j = 1 \quad (\text{A.8})$$

where  $m$  is an arbitrary constant. As plugging  $\xi_j = m/|\alpha_j|$  (from Eq.(A.7)) into Eq.(A.8), Eq.(A.9) can be derived.

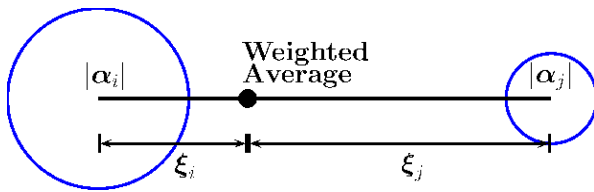


Fig. B.17. Graphical illustration of weight coefficient calculation.

$$\xi_i = 1 - \frac{m}{|\alpha_i|} \quad (A.9)$$

Because  $\xi_i = m/|\alpha_i|$ ,

$$\frac{m}{|\alpha_i|} = 1 - \frac{m}{|\alpha_j|} \quad \text{and} \quad m = \frac{|\alpha_i||\alpha_j|}{|\alpha_i| + |\alpha_j|} \quad (A.10)$$

Thus, the weight coefficients can be derived:

$$\xi_i = \frac{|\alpha_j|}{|\alpha_i| + |\alpha_j|} \quad (A.11)$$

$$\xi_j = \frac{|\alpha_i|}{|\alpha_i| + |\alpha_j|} \quad (A.12)$$

Note that the inequality,  $\xi_i < \xi_j$ , holds if  $|\alpha_i| > |\alpha_j|$ .

## References

- [1] Wade H. Volume, shape, and roundness of quartz particles. *J Geol* 1935;43(3): 250–80.
- [2] Krumbein WC. Measurement and geological significance of shape and roundness of sedimentary particles. *J Sediment Petrol* 1941;11(2):64–72.
- [3] Zwing T. Beitrag zur Schotteranalyse. ETH Zürich; 1935.
- [4] Albanese A, Tang PS, Chan Warren CW. The effect of nanoparticle size, shape, and surface chemistry on biological systems. *Ann Rev Biomed Eng* 2012;14:1–16.
- [5] Wagner J, Ghosal S, Whitedeck T, Metayer C. Morphology, spatial distribution, and concentration of flame retardants in consumer products and environmental dusts using electron microscopy and raman micro-spectroscopy. *Environ Int* 2013;59:16–26.
- [6] DeCarlo PF, Sflowik JG, Worsnop DR, Davidovits P, Jimenez JL. Particle morphology and density characterization by combined mobility and aerodynamic diameter measurements. part 1: Theory. *Aerosol Sci Technol* 2004;38(12): 1185–205.
- [7] Stanford MK, DeSilvaCorte C, Eylon D. Effect of particle morphology on flow characteristics of a composite plasma spray powder. *J Therm Spray Technol* 2004; 13(4):586–92.
- [8] Barandiaran M, Dfickerson JH. Nanoscale engineering of  $\text{TiO}_2$  nanoparticles: Evolution of the shape, phase, morphology, and facet orientation. *Mater Lett* 2016; 180:212–8.
- [9] Vafdes-Vidal G, Caflabi-Floody A, Miro-Recasens R, Norambuena-Contreras J. Mechanical behavior of asphalt mixtures with different aggregate type. *Constr Build Mater* 2015;101(Part 1):474–81.
- [10] Buflord JW, Garboczi EJ. Defining shape measures for 3d star-shaped particles: Sphericity, roundness, and dimensions. *Powder Technol* 2013;249:241–52.
- [11] Taylor MA, Garboczi EJ, Erdogan ST, Fowler DW. Some properties of irregular 3-d particles. *Powder Technol* 2006;162(1):1–15.
- [12] Blott SJ, Pye K. Particle shape: a review and new methods of characterization and classification. *Sedimentology* 2008;55(1):31–63.
- [13] Rodriguez JM, Edeskar T, Knutson S. Particle shape quantifies and measurement techniques - a review. *The. Electron J Geotech Eng* 2013;18(A):169–98.
- [14] Zhou B, Wang J, Wang H. Three-dimensional sphericity, roundness and fractal dimension of sand particles. *Geotechnique* 2018;68(1):18–30.
- [15] Sukumaran B. Quantitative characterisation of the geometry of discrete particles. *Geotechnique* 2001;51(7):619–27.
- [16] Tutumcu E, Rao C, Stefanek JA. Videoframe analysis of aggregate. Tech. Rep. FHWA-HIF-11-030. University of Illinois at Urbana-Champaign, Urbana, Illinois, The Federal Highway Administration, The Illinois Department of Transportation; July 2000.
- [17] Bagheri GH, Bonadonna C, Manzefi I, Vonlanthen P. On the characterization of size and shape of irregular particles. *Powder Technol* 2015;270(Part A):141–53.
- [18] Akhmetli KA, Druckrey AM, Al-Raoush RI, Weiskittel T, Lavrik NV. Quantifying morphology of sands using 3D imaging. *J Mater Civ Eng* 2015;27(10):1–10.
- [19] Zhang C, Zhao S, Zhao J, Zhou X. Three-dimensional voronoi analysis of realistic granular packing: An octree-based voronoi tessellation framework. *Powder Technol* 2021;379:251–64.
- [20] Gates L, Masad E, Pye R, Bushee D. Aggregate imaging measurement system 2 (aims2): Final report. Tech. Rep. FHWA-HIF-11-030, Federal Highway Administration, U.S. Department of Transportation, 1200 New Jersey Avenue, SE, Washington DC 20590, Highways for LIFE Technology Partnership Program; January 2011.
- [21] Wang L, Sun W, Tutumcu E, Drata C. Evaluation of aggregate imaging techniques for quantification of morphological characteristics. *J Transp Res Board* 2013;2335: 39–49.
- [22] Liang Z, Nie Z, An A, Gong J, Wang X. A particle shape extraction and evaluation method using a deep convolutional neural network and digital image processing. *Powder Technol* 2019;353:156–70.
- [23] Ifizuka K. Engineering Optics. 4th ed. Springer; 2019.
- [24] Liebold F, Maas HG, Deutsch J. Photogrammetric determination of 3D crack opening vectors from 3D displacement fields. *ISPRS J Photogram Remote Sens* 2020;164:1–10.
- [25] Giancola S, Vafentzi M, Safla R. A Survey on 3D Cameras: Metrological Comparison of Time-of-Flight, Structured-Light and Active Stereoscopy Technologies. Springer; 2018.
- [26] Wade H. Volume, shape, and roundness of rock particles. *J Geol* 1932;40(5): 443–51.
- [27] Sneed ED, Folk RL. Pebbles in the Colorado River, Texas: a study in particle morphology. *J Geol* 1958;66(2):114–50.
- [28] Huang H, Luo J, Tutumcu E, Hart JM, Stofla AJ. Automated segmentation and morphological analyses of stockpile aggregate images using deep convolutional neural networks. *Transp Res Rec* 2020;2674(10):285–98.
- [29] Huang H, Luo J, Qamhia I, Tutumcu E, Hart JM, Stofla AJ. I-rifrap computer vision software for automated size and shape characterization of rifrap in stockpile images. *Transp Res Rec* 2021;2675(9):238–50.
- [30] Zheng J, Hryciw RD. Roundness and sphericity of soil particles in assemblies by computational geometry. *J Comput Civ Eng* 2016;30(6):1–13.
- [31] Wu H-L, Yu J, Zhang D, Zheng J-X, Li VC. Effect of morphological parameters of natural sand on mechanical properties of engineered cementitious composites. *Cement Concr Compos* 2019;100:108–19.
- [32] Berreux E, Cuervas-Mons J, Rodriguez-Rey Ángeles, Ordóñez-Casado B. Representativity of 2d shape parameters for mineral particles in quantitative petrography. *Minerals* 2019;9(12):768.
- [33] Vangla P, Roy N, Gaffi ML. Image based shape characterization of granular materials and its effect on kinematics of particle motion. *Granular Matter* 2018;20(6).
- [34] Wang L, Wang X, Mohammad I, Abadie C. Unified method to quantify aggregate shape angularity and texture using fourier analysis. *J Mater Civ Eng* 2005;17(5): 498–504.
- [35] Su D, Yan WM. Prediction of 3D size and shape descriptors of irregular granular particles from projected 2D images. *Acta Geotech* 2020;15:1533–55.
- [36] Maroof MA, Mahboubi A, Noorzad A, Saffi Y. A new approach to particle shape classification of granular materials. *Transp Geotech* 2020;22:100296.
- [37] Wade H. Sphericity and roundness of rock particles. *J Geol* 1933;41(3):310–31.
- [38] Lee SJ, Lee CH, Shin M, Bhattacharya S, Su YF. Influence of coarse aggregate angularity on the mechanical performance of cement-based materials. *Constr Build Mater* 2019;204:184–92.
- [39] Maroof MA, Mahboubi A, Noorzad A. A new method to determine specific surface area and shape coefficient of a cohesionless granular medium. *Adv Powder Technol* 2020;31(7):3038–49.

- [40] Kuang D, Zhang B, Jifiao Y, Fang J, Chen H, Wang L. Impact of particle morphology on aggregate-asphalt interface behavior. *Constr Build Mater* 2017;132:142–9.
- [41] Su YF, Bhattacharya S, Lee SJ, Lee CH, Shfin M. A new interpretation of three-dimensional particle geometry: M-A-V-L. *Transp Geotech* 2020;23:100328.
- [42] Garboczi EJ. Three-dimensional mathematical analysis of particle shape using x-ray tomography and spherical harmonics: Application to aggregates used in concrete. *Cem Concr Res* 2002;32(10):1621–38.
- [43] Takashimizu Y, Ifiyoshi M. New parameter of roundness R: Circularity corrected by aspect ratio. *Prog Earth Planetary Sci* 2016;3(2).
- [44] Prasad S, Schweizer C, Bagaria P, Kufatulika WD, Mashuga CV. Effect of particle morphology on dust cloud dynamics. *Powder Technol* 2017;379:89–95.
- [45] Cho G-C, Dodds J, Santamarina JC. Particle shape effects on packing density, stiffness, and strength: Natural and crushed sands. *J Geotech Geoenviron Eng* 2006;132(5):591–602.
- [46] Lee CH, Shfin M, Lee SJ. Interrelation of morphological findings and 2-d generalized regularity for coarse aggregate in cement-based materials. *Constr Build Mater* 2020;251:118984.
- [47] Robert CP, Casella G. *Monte Carlo Statistical Methods*. 2nd ed. USA: Springer; 2004.
- [48] ASTM D 4791-19. Standard Test Method for Flat Particles, Elongated Particles, or Flat and Elongated Particles in Coarse Aggregate. ASTM International, West Conshohocken, PA; 2019.
- [49] Poflyga, Poflyga Compact C504; 2021. URL: <https://www.poflyga.com/products/compact-c504/> [accessed: 2021-04-14].
- [50] Muthén LK, Muthén BO. How to use a monte carlo study to decide on sample size and determine power. *Struct Equ Model* 2002;9(4):599–620.
- [51] Safliby E. Descriptive sampling: A better approach to monte carlo simulation. *J Oper Res Soc* 1990;41(12):1133–42.
- [52] Zheng J, Hryciw RD. Traditional soil particle sphericity, roundness and surface roughness by computational geometry. *Geotechnique* 2015;65(6):494–506.
- [53] Hardle WK, Stoffer D. *Applied Multivariate Statistical Analysis*. 4th ed. Springer; 2015.
- [54] Adachi K. *Matrix-Based Introduction to Multivariate Data Analysis*. Springer; 2016.
- [55] Kline RB. *Principles and Practice of Structural Equation Modeling*. 3rd ed. The Guilford Press; 2011.
- [56] Patel A, Bartak PP, Singh DN. An empirical relationship for determining shear wave velocity in granular materials accounting for grain morphology. *Geotech Test J* 2009;32(1):1–10.
- [57] R Core Team. R: A Language and Environment for Statistical Computing, R Foundation for Statistical Computing, Vienna, Austria; 2020. URL: <http://www.R-project.org/>.
- [58] Roseefl Y. lavaan: An R package for structural equation modeling. *J Statistical Software* 2012;48(2):1–36. URL: <http://www.jstatsoft.org/v48/i02/>.
- [59] Tse Hu L, Bentler PM. Cutoff criteria for fit indexes in covariance structure analysis: Conventional criteria versus new alternatives. *Struct Equ Model* 1999;6(1):1–55.